Precision high-value resistance scaling with a two-terminal cryogenic current comparator

F. L. Hernandez-Marquez', M. E. Bierzychudek', G. R. Jones Jr., and R. E. Elmquist'

Citation: Rev. Sci. Instrum. **85**, 044701 (2014); doi: 10.1063/1.4869240
View online: http://dx.doi.org/10.1063/1.4869240
View Table of Contents: http://aip.scitation.org/toc/rsi/85/4
Published by the American Institute of Physics

Precision high-value resistance scaling with a two-terminal cryogenic current comparator

F. L. Hernandez-Marquez,[1,a)] M. E. Bierzychudek,[2,a)] G. R. Jones, Jr.,[3] and R. E. Elmquist[3,b)]
[1]*Centro Nacional de Metrología, Querétaro 76900, Mexico*
[2]*Instituto Nacional de Tecnología Industrial, San Martin, Buenos Aires B1650WAB, Argentina*
[3]*National Institute of Standards and Technology, Gaithersburg, Maryland 20899-8171, USA*

(Received 30 September 2013; accepted 1 March 2014; published online 4 April 2014)

We describe a cryogenic two-terminal high-resistance bridge and its application in precision resistance scaling from the quantized Hall resistance (QHR) at $R_H = R_K/2 = 12\,906.4035\ \Omega$ to decade resistance standards with values between 1 MΩ and 1 GΩ. The design minimizes lead resistance errors with multiterminal connections to the QHR device. A single variable voltage source and resistive ratio windings are utilized to achieve excellent dynamic stability, which is not readily obtained in low-current measurements with conventional cryogenic current comparators (CCCs). Prototypes of this bridge have been verified by a successful international comparison of high-resistance scaling using two-terminal CCCs in the national metrology institutes of Argentina, Mexico, and the United States. © *2014 AIP Publishing LLC*. [http://dx.doi.org/10.1063/1.4869240]

I. INTRODUCTION

High resistance standards are necessary for traceable measurements of small dc currents, for example, to monitor ionizing radiation, aerosols, leakage currents, and biochemical processes. Precision high resistance scaling processes (which build up from lower to higher resistance values) can be limited by uncertainty due to electrical leakage and noise in the current detection system. The conventional methods of resistance scaling in this range are Hamon devices, based on series-parallel high-resistance networks,[1] and potentiometric bridges that use series resistive dividers or dual voltage sources.[2] Carefully constructed guarded Hamon devices are capable of low uncertainties but their use requires considerable investment in time and in the standards themselves. With the exception of the Josephson potentiometer,[3] dc potentiometric bridges have an uncertainty that is determined by other resistance or voltage artifacts, and instability in these references may limit their uncertainty levels.

Modern resistance bridge designs strive to minimize the requirements of direct operator control and to utilize various compensation and balancing techniques to provide high accuracy and measurement efficiency. Cryogenic current comparators (CCCs)[4] achieve unmatched sensitivity (exceeding one part in 10^9 for some resistance values) in determining resistance ratios using dc currents,[5,6] and some have been commercialized for use in the traceability of primary metrology standards based on the quantized Hall resistance (QHR) standard.[7,8] CCCs use the high magnetic flux sensitivity of superconducting quantum interference devices (SQUIDs) as a means of sensing and maintaining a precise bridge current ratio. The energizing currents in conventional four-terminal CCC bridges are supplied by two isolated ramping current sources.[9] The SQUID senses the current balance as describe in Sec. II and provides feedback to maintain the current ratio. The dynamic balance of the SQUID feedback circuits is notoriously difficult to maintain given the limited range of linearity and output bandwidth provided by commercial SQUID magnetometers. This problem becomes more acute if the number of turns in the windings must be increased to be sensitive to smaller currents as this also results in larger self-inductance.[10,11] These are sources of concern in CCC design and have limited the widespread use of CCCs, especially for high resistance.[12,13]

Early two-terminal CCC systems were developed in the 1970s to compare cryogenic resistors used in voltage ratio dividers.[14,15] These bridges could measure large resistance ratios and allowed low-voltage Josephson standards consisting of only a few junctions to be compared to 1.018 V standard Weston cells for precise voltage metrology. They were displaced by Josephson junction arrays[16] that did not require voltage scaling and later restored for use in the measurement of small currents based on the QHR.[10] Here we describe the use of recently designed two-terminal CCCs for comparisons based on the QHR standard and for resistance scaling as high as 1 GΩ. We find that this method provides excellent stability with good sensitivity to small currents and allows low uncertainty in high-value resistance measurements. SQUID stability issues can be overcome by two-terminal CCCs because current is supplied by a single voltage source, eliminating the need to correct for the deviations in dual-source tracking.

II. CCC BALANCE OPERATION

In most modern CCCs magnetic flux is generated by two or more current-carrying windings inside a shield[14] consisting

[a)]F. Hernandez-Marquez and M. Bierzychudek contributed as Foreign Guest Researchers in the design and construction phases of this work, performed at the National Institute of Standards and Technology. Their contributions to the measurements were made at their own institutes.
[b)]Author to whom correspondence should be addressed. Electronic mail: relmquist@nist.gov

of a continuous self-enclosing superconducting foil sheath, usually made of lead. This self-enclosing toroidal shield is a more compact form of an isolated, long, and narrow superconducting tube which strongly attenuates the leakage of residual flux that might depend on the relative position of the windings. For each enclosed winding N indicated by subscript j, N_j is the number of turns, and I_j is the (directional) current. A shielding current I_T equal to the sum of the ampere-turns products of all enclosed windings flows parallel to the windings around the shield on its inner surface,

$$I_T = \sum N_j I_j. \tag{1}$$

Due to the Meissner effect this shielding current cannot penetrate directly through the superconductor. By isolating the self-enclosing shield layers, we ensure that this net dc current circulates without attenuation along the inside and outside shield surfaces in a closed loop.

In the CCC bridge, the current in windings N_1 and N_2 produces nearly cancelling magnetic flux and thus the net result is only a small shielding current. This can be efficiently coupled to a SQUID magnetometer pick-up coil using a superconducting flux transformer and the resulting SQUID signal $S(I)$ can provide the basis for feedback. In the four-terminal CCC (see Fig. 1) the SQUID signal provides an additive compensation current I_C in one main bridge arm that drives the SQUID output to zero. A sensitive voltmeter detects the imbalance in voltage between the two resistors and this signal may be used to calculate the precise resistance ratio. Alternatively, the voltage detector's signal can generate a secondary feedback current I_F through a third winding N_F, which is measured across resistor R_F. In the final balance condition of the bridge shown in Fig. 1 the SQUID signal is brought to zero,

$$S(I) = I_1 N_1 - (I_2 + I_C) N_2 + I_F N_F + \Delta = 0. \tag{2}$$

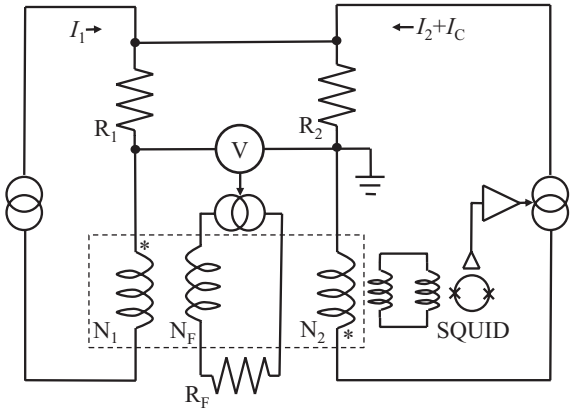

FIG. 1. Diagram of a four-terminal CCC bridge used to compare resistors R_1 and R_2. Windings N_1, N_F, and N_2 are located inside a self-enclosing superconducting shield (dashed box). Two main currents I_1 and $I_2 + I_C$ are generated in a precise integer ratio in two standards resistors R_1 and R_2. The voltage across the resistors is measured by the nanovolt detector V, and feedback is supplied to a third winding in order to balance the nanovolt detector signal.

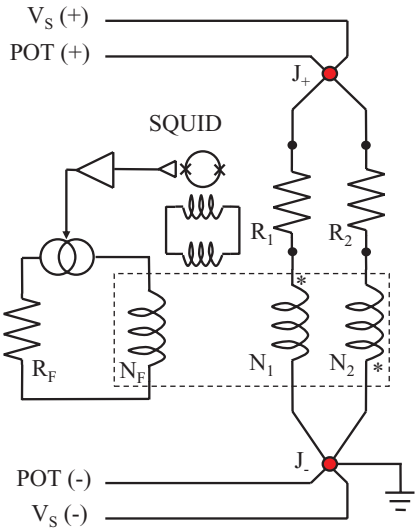

FIG. 2. Diagram of a basic two-terminal CCC bridge in which resistors R_1 and R_2 are compared. Windings N_F, N_1, and N_2 are enclosed in a self-enclosing superconducting shield (dashed box). Junctions J_+ and J_- define a potential difference that is the same for the two arms of the bridge. Any resistance in series with a standard resistor between these junctions contributes to a summed resistance correction r_{w1} or r_{w2}.

Here the current gain factor has been set equal to one and the term Δ accounts for the zero offset of the SQUID signal when there is no net flux generated by the CCC windings.

In the two-terminal CCC design, shown in Fig. 2, voltage balance is achieved by the single voltage source that energizes both arms of the bridge. The SQUID signal is applied not as compensation to one of the main currents but as a feedback current I_F to a third, independent winding N_F, which is usually a single turn ($N_F = 1$). The SQUID balance condition is given by

$$S(I) = I_1 N_1 - I_2 N_2 + I_F N_F + \Delta = 0. \tag{3}$$

Note that the main currents in any type of CCC bridge should be simultaneously reversed in polarity to measure the difference $S(I_+) - S(I_-)$, so as to eliminate the offset Δ.

The following equations define the currents I_1 and I_2 that appear in (3), where R_1 and R_2 are the values of the standard resistors and V_S is the source voltage between the bridge connection points J_+ and J_-:

$$I_1 = \frac{V_S}{R_1 + r_{w1}}, \quad I_2 = \frac{V_S}{R_2 + r_{w2}}. \tag{4}$$

Calculation of the unknown resistor's value requires measuring two resistance correction values r_w that appear in series with the standard resistors. These include the resistance of leads and windings between junctions J_+ and J_-, and relative to R_1 and R_2 these are quite small. The resistance corrections for high-value resistors ($R \geq 1$ MΩ) can be measured to produce a relative uncertainty of less than 10^{-8}.[17] We solve the bridge Eqs. (3) and (4) above to find the unknown resistance R_1,

$$R_1 = \frac{V_S N_1}{V_S N_2/(R_2 + r_{w2}) - I_F N_F} - r_{w1}. \tag{5}$$

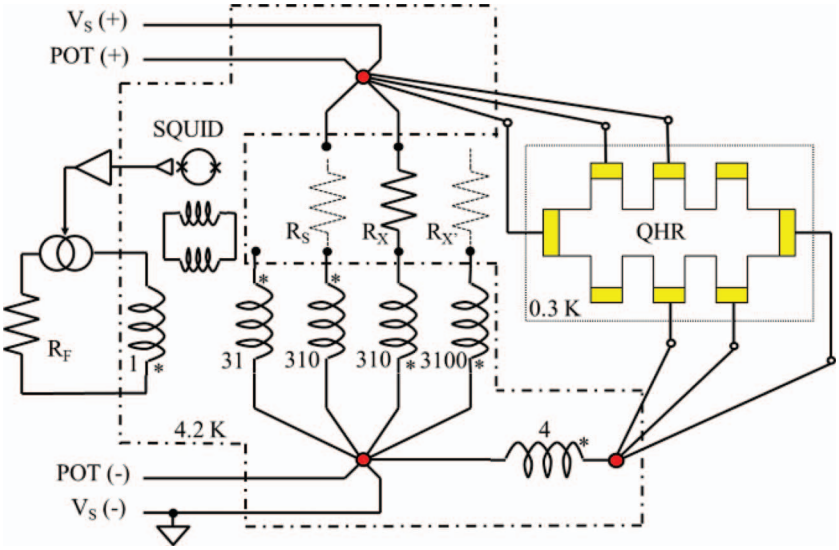

FIG. 3. Diagram of a two-terminal CCC bridge used for high resistance scaling. The cryogenic region inside the CCC cryostat is delineated by a dashed-dotted line and the CCC superconducting shield is omitted in this drawing. Several scaling configurations are possible. A QHR device can serve as a reference (as shown). Room-temperature standard resistors then occupy only one of the positions marked R_X or $R_{X'}$. Alternatively a room-temperature standard can serve as the reference resistor R_S with 31 turns or 310 turns to scale to higher decade-value resistance standards R_X or $R_{X'}$. Superconducting junctions are shown as larger filled circles.

A complete diagram of the two-terminal CCC is shown in Fig. 3. Four ratio windings of phosphor-bronze wire are used in series with standard resistors, and have 31, 310, 310, and 3100 turns. The QHE device is used with a winding of four turns. For high sensitivity, the two-terminal CCC winding set has an inner diameter of greater than 5 cm and as a result there is significant and unavoidable self-inductance in the winding of 3100 turns. The distributed resistance provided by the phosphor-bronze wire damps resonances[10] in this winding that otherwise can destabilize the SQUID. The winding resistance also serves to bring the level of the bridge feedback current close to zero for standard resistors close to the nominal values. For example, when a resistance of exactly 1 MΩ is balanced against the QHR standard the ratio value is smaller than the winding ratio of 310/4 = 77.5 by about 246×10^{-6} (in relative units). The resistance ratio $(R_1 + r_{w1})/(R_K/2)$ is brought close to the winding ratio when the bridge arm has a total resistance of approximately 1 000 246 Ω for the 310-turn winding or 10 002 460 Ω for the 3100-turn winding.

The junctions J_+ and J_- at the terminations of the arms of the bridge and the QHR connections are superconducting in order to eliminate spreading resistance, and the four-turn winding used with the QHR is made of superconducting NbTi wire. Section III describes how multiple QHR device leads as shown in Fig. 3, combined with the above superconducting circuit elements, can produce a near-zero lead resistance correction relative to the value of the QHR standard.

III. MINIMIZING QHR LEAD RESISTANCE ERROR

A unique property of the quantum Hall effect (QHE) allows the plateau resistance to be measured accurately in a two-terminal configuration with negligible lead resistance correction. This can be made clear if one considers the circuit of Fig. 4, where the QHR device has approximately zero longitudinal resistivity when supplied with an external current I_T and is suitable for precision metrology.[18] Due to the Lorentz force and the QHE, current that traverses the device through the source and drain contacts maintains a voltage $V_H = V_+ - V_-$ between the intermediate terminals of the device. Thus as long as all contacts have low contact resistance, $R_C \ll R_H$, a "guarding" voltage inhibits current from entering the device at the side contacts in the circuit of Fig. 4. The side contacts, especially those farthest from the source and drain, carry negligible current. A similar technique is described in Ref. 19 whereby multiple links are used to connect QHR devices together to obtain precise multiples or submultiples of individual quantized Hall resistances. The two-terminal resistance of this device connection differs from R_H by a relative error of order $(R_C/R_H)^M$ where M is the number of external leads connected to discrete high or low device contacts.[20,21] For $M = 3$, $R_C \leq 10$ Ω, and $R_H = R_K/2$, the resulting resistance value differs from the conventional four-terminal QHR resistance value by less than one part in 10^9.

In practice the two-terminal CCC and the QHR device reside in separate cryostats. Six non-superconducting leads with resistance ≈ 5 Ω are connected to the QHR device. Each

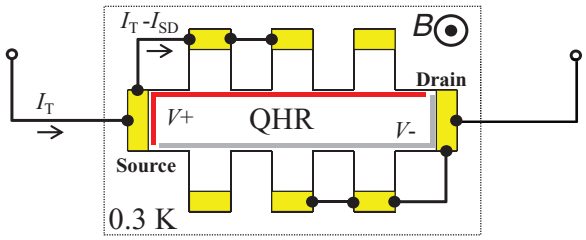

FIG. 4. A local two-terminal connection for an ideal QHR device, with near-zero longitudinal resistivity. The contacts on the narrower ends of the device are the source and drain and all contacts have equal contact resistance R_C. For $R_C \ll R_H$ the source-drain current is $I_{SD} \approx I_T$.

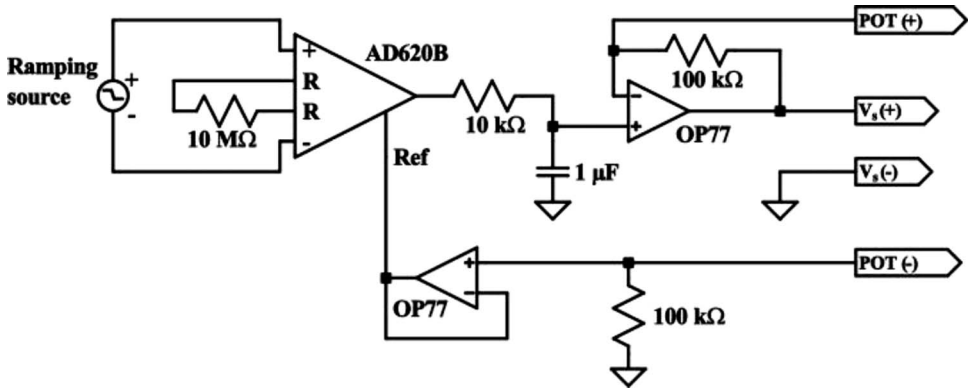

FIG. 5. Schematic diagram of the ramping voltage source output stage.

of the six normal conducting QHR leads is in series with a contact resistance R_C, and as described above the effective resistance due to this connection scheme is negligible when each connection has series resistance below 10 Ω. All major bridge circuit junctions are made in the liquid helium bath of the CCC cryostat.

IV. MEASUREMENT PROCESS

At the beginning of a group of measurements, resistance corrections r_{w1} and r_{w2} are determined by removing all standards from the bridge, placing an electrical short in the circuit position of one standard resistor, and measuring the four-terminal resistance between the J_+ and J_- voltage source junctions. This is repeated for each winding to determine the necessary resistance corrections. The first set of resistors under test is then connected and the source voltage is measured at the source junctions. After SQUID feedback is activated the source voltage is ramped between polarities. The bridge feedback system is very stable and can maintain lock throughout this reversal even in the presence of significant noise due to external interference. The feedback current (I_F) is derived from the analog output of a commercial dc SQUID system and measured across a precision wire-wound 200 kΩ resistor. Measurements of the voltage across the feedback resistor R_F are collected in sets for each voltage polarity using a time-symmetric sequence. This sequence includes two voltage reversals typically separated by 20–40 s, allowing delays for settling. This measurement eliminates linear drift in the SQUID circuit and thermally induced offset voltages in the bridge. All of these functions are performed using a sensitive digital multimeter through a USB IEEE-488 interface and personal computer. Each ratio comparison typically requires about 15–30 min to reach a minimum level of total uncertainty, dominated by type B systematic influences. Influences on the measurement uncertainty have been described and estimated;[17] the most significant is the low-frequency noise of the CCC/SQUID detection circuit for high resistance values greater than 1 MΩ.

The CCC electronics system is battery-powered and includes three circuit boards housed in one unit. A solid-state voltage reference provides long-term stability for the main voltage source. The linear voltage ramp is produced using a digital circuit[9] and polarity reversal is applied to the voltage signal by relays. The voltage source produces an output of ±0.5 V to ±1.1 V for use with the QHR, since typical QHR devices are likely to have longitudinal resistance that is nonzero for higher current levels. Source output levels of ±5 V or ±10 V are used when room-temperature standard resistors are compared. The analog output circuit, shown in Fig. 5, filters the output and corrects for any voltage drop in the leads using remote sensing at the bridge arm junctions.

V. INTERNATIONAL COMPARISON OF HIGH RESISTANCE

Two-terminal CCC bridges for resistance scaling were designed and constructed at NIST with the support of visiting staff from three other NMIs: the Centro Nacional de Metrología – Mexico (CENAM), the National Measurement Institute – Australia (NMIA), and the Instituto Nacional de Tecnología Industrial – Argentina (INTI). Each institute obtained one prototype bridge as in Fig. 3, designed for high-resistance scaling. These bridges were identical except in minor ways, such as the exact values of the winding resistances. An international comparison of high value resistance standards was performed in 2012 with the purpose of comparing the high resistance CCC scaling of the participating NMIs using these bridges. This comparison involved three of the cooperating labs, all of which are members of the Sistema Interamericano de Metrologia (SIM) Regional Metrology Organization (RMO) and was officially sanctioned within the SIM RMO as comparison SIM.EM-S10.

In order to provide a complete evaluation of the systems and redundancy at each resistance level, two traveling standards of each decade value between 1 MΩ and 1 GΩ were selected. These resistors were NIST-constructed hermetically sealed film-type standards[22] or commercial standards of similar construction and quality. The resistors were selected to have low and linear drift, low temperature coefficient of resistance (TCR), low voltage coefficient, and negligible settling time.[23] The scaling process was based on QHR standards maintained in each of the laboratories. NIST measured the 1 MΩ standards directly against the QHR at or below 1.1 V, and then scaled between the high resistance traveling standards using a source voltage of 10 V. At CENAM and INTI scaling was initiated using 10 kΩ reference standards,

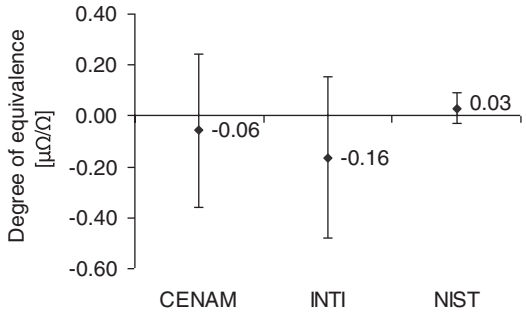

FIG. 6. Combined results for two traveling resistance standards at the 1 MΩ level, showing the degree of equivalence with respect to the CRV and its expanded uncertainty ($k = 2$) represented with the errors bars. Relative differences from the time-dependent comparison reference value are given beside each point in $\mu\Omega/\Omega$. (Reprint with permission from M. Bierzechudek, R. E. Elmquist, and F. Hernandez, SIM.EM-S10 RMO Comparison Final Report, pp. 9–10, Aug. 2013. Copyright 2013 BIPM, which retains full internationally protected copyright.)[25]

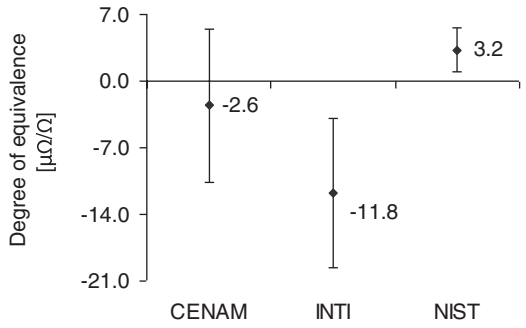

FIG. 7. Combined results for two traveling resistance standards at the 1 GΩ level, showing the degree of equivalence with respect to the CRV and its expanded uncertainty ($k = 2$) represented with the errors bars. Relative differences from the time-dependent comparison reference value are given beside each point in $\mu\Omega/\Omega$. (Reprint with permission from M. Bierzechudek, R. E. Elmquist, and F. Hernandez, SIM.EM-S10 RMO Comparison Final Report, pp. 11–12, Aug. 2013. Copyright 2013 BIPM, which retains full internationally protected copyright.)[26]

calibrated against the QHR, followed by scaling from 10 kΩ to 1 MΩ and higher values using the two-terminal CCC at 10 V. The use of 5 V was necessary at INTI for the initial scaling from 10 kΩ to 1 MΩ resistors because their prototype has winding resistances that were not closely enough matched, and the SQUID feedback range is insufficient to accommodate the flux excursion at 10 V (see Sec. II). Each NMI measured the resistors over a period of two to four weeks, allowing one week for recovery from the effects of transport by commercial carriers. The results were adjusted for the temperature deviation, using the TCR of each standard. The temperature uncertainty was between 0.05 °C and 0.1 °C, depending the laboratory This generates one of the larger uncertainty components in the resistance comparisons at and above 100 MΩ. The final results were analyzed using a standard method[24] that eliminates the linear drift in each resistor's value based on repeated measurements by one of the laboratories.

Results of the 1 MΩ and 1 GΩ comparisons from SIM.EM-S10 are presented in Figs. 6 and 7. Each graph shows the differences between NMIs, conventionally known as the degree of equivalence (DOE) with respect to the comparison reference value (CRV), at one resistance level along with the NMI-assigned standard uncertainty. The CRV is calculated as the weighted average of the combined difference relative to the time-estimated value for each institute; see Ref. 24 for more information. To provide a broad overview of the results, Table I gives a summary of the SIM.EM-S10 DOE and standard uncertainty at each resistance level. These may be compared with similar results from two other recent international comparisons and with the calibration measurement capabilities (CMCs)[23] as reported to the International Bureau of Weights and Measures (BIPM). These CMCs describe the uncertainty levels that each NMI uses in traceable calibrations for customers. The international comparisons are

TABLE I. Recent international comparison results and CMC uncertainties for the three participating NMIs. All uncertainty values have a coverage factor of $k = 2$.

	CENAM		INTI		NIST	
Participating NMI	DOE ($\mu\Omega/\Omega$)	Uncertainty ($k = 2$, $\mu\Omega/\Omega$)	DOE ($\mu\Omega/\Omega$)	Uncertainty ($k = 2$, $\mu\Omega/\Omega$)	DOE ($\mu\Omega/\Omega$)	Uncertainty ($k = 2$, $\mu\Omega/\Omega$)
			1 MΩ			
SIM.EM-S10	− 0.06	0.30	− 0.16	0.32	0.03	0.06
SIM.EM-S6	0.30	0.39	− 2.73	1.08	0.01	0.01
CMC uncertainty		1.5		2.5		0.2
			10 MΩ			
SIM.EM-S10	0.81	0.58	− 0.15	0.50	− 0.05	0.08
CCEM-K2	…[a]		…[a]		− 0.3	2.9
CMC uncertainty		10		4		3
			100 MΩ			
SIM.EM-S10	0.6	1.7	− 2.7	1.8	0.2	0.3
CMC uncertainty		15		7		5
			1 GΩ			
SIM.EM-S10	− 2.6	8.0	− 11.8	7.8	3.2	2.3
SIM.EM-K2	3.6	6.9	− 7.6	4.8	0.7	0.4
CCEM-K2	…[a]		…[a]		− 0.1	8.6
CMC uncertainty		20		10		10

[a]Neither CENAM nor INTI participated in the CCEM-K2 comparison.

the 2007–2008 SIM.EM-S6/K2 comparisons at the 1 MΩ and 1 GΩ[23] and the 1996–2000 CCEM-K2 comparison at 10 MΩ and 1 GΩ[22,23] conducted under the direction of the Consultative Committee on Electricity and Magnetism (CCEM). NIST served as the pilot laboratory and made multiple measurement contributions in all of the listed comparisons, and thus its results carry a relatively larger weight than other NMIs in the calculations of the CRVs and this reduces the NIST DOEs.

The results at the 1 MΩ through 100 MΩ levels help to improve traceability by reducing the uncertainty of dc resistance measurements as well as to improve the agreement among the participating laboratories for international equivalence. The results at 1 GΩ are somewhat less useful, since most values show an increase from earlier results in both the degree of equivalence and their uncertainty. The SIM.EM-K2 comparison, however, was based on Hamon scaling and conventional methods that utilized an applied voltage of typically 100 V, while in the present CCC comparison the applied voltage was 10 V. This lower voltage reduces the CCC sensitivity and dominates the CCC measurement uncertainty for scaling of resistance values above 100 MΩ.[17]

VI. CONCLUSIONS

We have developed a two-terminal CCC measurement system that can be used effectively for improved scaling with high-resistance standards, reducing the measurement time and improving the uncertainty at low voltage compared with conventional methods. With this two-terminal CCC bridge design a unique low-current resolution is obtained from high-inductance, resistive windings. The design eliminates the use of a sensitive nanovolt detector and operates with a single grounded source, which helps to reduce noise and improves the dynamic stability relative to traditional four-terminal CCCs. Three prototypes of this system were successfully and independently operated in three NMI laboratories and we reported the results of a SIM RMO comparison of high-value resistors between 1 MΩ and 1 GΩ based on QHR standards. These results are consistent with substantial reductions in the scaling uncertainties of those NMIs using two-terminal high-resistance CCC systems.

ACKNOWLEDGMENTS

The authors would like to thank B. Rodríguez, who helped to perform the measurements at CENAM, M. Curras, R. Iuzzolino, A. Tonina and M. Real, who helped to perform the measurements at INTI, D. Jarrett and M. Kraft, who helped to characterize the resistors at NIST, B. J. Pritchard, formerly of NMI – Australia, who contributed to the scaling CCC design, and Chun-Feng Huang, formerly of ITRI – Taiwan, who provided QHR samples.

[1] D. G. Jarrett, IEEE Trans. Instrum. Meas. **48**, 324–328 (1999).
[2] D. G. Jarrett, IEEE Trans. Instrum. Meas. **50**, 249–254 (2001).
[3] T. Endo, Y. Murayama, M. Koyanagi, J. Kinoshita, K. Inagaki, C. Yamanouchi, and K. Yoshi, IEEE Trans. Instrum. Meas. **34**, 323–327 (1985).
[4] I. K. Harvey, Rev. Sci. Instrum. **43**, 1626–1629 (1972).
[5] T. J. Witt, Rev. Sci. Instrum. **69**, 2823–2843 (1998).
[6] J. M. Williams, IET Sci. Meas. Technol. **5**, 211–224 (2011).
[7] D. Drung, M. Goetz, E. Pesel, J.-H. Storm, C. Aßmann, M. Peters, and Th. Schurig, Supercond. Sci. Technol. **22**, 114004–114011 (2009).
[8] J. M. Williams, T. J. B. M. Janssen, G. Rietveld, and E. Houtzager, Metrologia **47**, 167–174 (2010).
[9] R. E. Elmquist and R. F. Dziuba, Rev. Sci. Instrum. **62**, 2457–2460 (1991).
[10] R. E. Elmquist, E. Hourdakis, D. G. Jarrett, and N. M. Zimmerman, IEEE Trans. Instrum. Meas. **54**, 525–528 (2005).
[11] G. Rietveld, P. de la Court, and H. van den Brom, IEEE Trans. Instrum. Meas. **58**, 1196–1201 (2009).
[12] E. Pesel, E. Schumacher, and P. Warnecke, IEEE Trans. Instrum. Meas. **44**, 273–275 (1995).
[13] N. E. Fletcher, J. M. Williams, and T. J. B. M. Janssen, *2000 Conference on CPEM Digest, Sydney, Australia* (IEEE, Piscataway, NJ 2000), pp. 482–483.
[14] R. F. Dziuba, B. F. Field, and T. F. Finnegan, IEEE Trans. Instrum. Meas. **23**, 264–267 (1974).
[15] I. K. Harvey, Metrologia **12**, 47–54 (1976).
[16] C. A. Hamilton, Rev. Sci. Instrum. **71**, 3611–3623 (2000).
[17] M. E. Bierzychudek and R. E. Elmquist, IEEE Trans. Instrum. Meas. **58**, 1170–1175 (2009).
[18] B. Jeckelmann and B. Jenneret, Rep. Prog. Phys. **64**, 1603–1655 (2001).
[19] F. Delahaye, J. Appl. Phys. **73**, 7914–7920 (1993).
[20] A. M. Jeffery, R. E. Elmquist, and M. E. Cage, J. Res. Natl. Inst. Stand. Technol. **100**, 677–685 (1995).
[21] K. von Klitzing, Philos. Trans. R. Soc. London A **363**, 2203–2219 (2005).
[22] R. F. Dziuba and D. G. Jarrett, IEEE Trans. Instrum. Meas. **48**, 333–337 (1999).
[23] See http://kcdb.bipm.org/default.asp for information about Key Comparison Data Base (results for SIM.EM-S10, SIM.EM-S6, SIM.EM-K2, CCEM-K2, and NMI CMC tables).
[24] N. F. Zhang, N. Sedransk, and D. G. Jarrett, IEEE Trans. Instrum. Meas. **52**, 491–494 (2003).
[25] M. Bierzechudek, R. E. Elmquist, and F. Hernandez, SIM.EM-S10 RMO COMPARISON FINAL REPORT (Aug. 2013) pp. 9–10, available online: http://www.bipm.org/utils/common/pdf/final_reports/EM/S10/SIM.EM-S10.pdf
[26] M. Bierzechudek, R. E. Elmquist, and F. Hernandez, SIM.EM-S10 RMO COMPARISON FINAL REPORT (Aug. 2013), pp. 11–12, available online: http://www.bipm.org/utils/common/pdf/final_reports/EM/S10/SIM.EM-S10.pdf